JCTC Journal of Chemical Theory and Computation

Article

pubs.acs.org/JCTC

Combining the Bethe–Salpeter Formalism with Time-Dependent DFT Excited-State Forces to Describe Optical Signatures: NBO Fluoroborates as Working Examples

Paul Boulanger,[†,#] Siwar Chibani,[‡,#] Boris Le Guennic,[¶] Ivan Duchemin,[§] Xavier Blase,*[,†,∥] and Denis Jacquemin*[,‡,⊥]

[†]CNRS, Inst NEEL, F-38042 Grenoble, France

[‡]Laboratoire CEISAM-UMR CNRS 6230, Université de Nantes, 2 Rue de la Houssinière, BP 92208, 44322 Nantes Cedex 3, France

[¶]Institut des Sciences Chimiques de Rennes, CNRS-Université de Rennes 1, 263, Av. du Général Leclerc, 35042 Rennes Cedex, France

[§]INAC, SP2M/L Sim, CEA/UJF Cedex 09, 38054 Grenoble, France

[∥]Université Grenoble Alpes, Inst NEEL, F-38042 Grenoble, France

[⊥]Institut Universitaire de France, 103, bd Saint-Michel, F-75005 Paris Cedex 05, France

Supporting Information

ABSTRACT: We propose to use a blend of methodologies to tackle a challenging case for quantum approaches: the simulation of the optical properties of asymmetric fluoroborate derivatives. Indeed, these dyes, which present a low-lying excited-state exhibiting a cyanine-like nature, are treated not only with the Time-Dependent Density Functional Theory (TD-DFT) method to determine both the structures and vibrational patterns but also with the Bethe–Salpeter approach to compute both the vertical absorption and emission energies. This combination allows us to obtain 0–0 energies with a significantly improved accuracy compared to the "raw" TD-DFT estimates. We also discuss the impact of various declinations of the Polarizable Continuum Model (linear-response, corrected linear-response, and state-specific models) on the obtained accuracy.

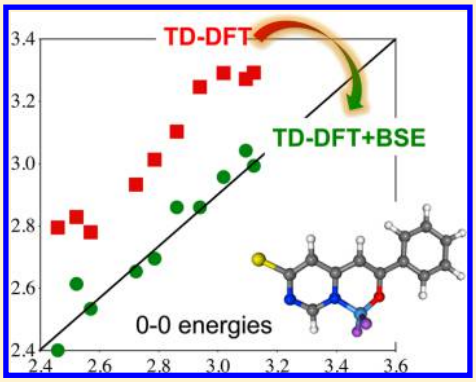

INTRODUCTION

For electronic excited-state (ES) calculations, reaching physically well-grounded comparisons between experimental and theoretical data remains difficult especially when "real-life" solvated molecules are considered. To date, most ES calculations are still performed in the so-called vertical approximation, that is, using a frozen structure typically the optimal ground-state (GS) geometry. While this approach certainly allows to obtain relevant chemical insights as well as to analyze trends in a homologous series of compounds,[1] it does not grant access to direct comparisons with experimental data, since vertical transition energies are not easily deduced from measured absorption and fluorescence spectra. It is rather usual in the theoretical dye chemistry field to directly compare experimental wavelengths of maximal absorption (λ_{max}) to vertical absorption energies,[1,2] but this scheme completely neglects vibrational effects and implies quite drastic approximations. On the bright side, obtaining vertical values only requires the computation of transition energies from the GS to a given ES, and this allows one to take advantage of a well-stocked toolbox of quantum methods, including highly correlated wave function schemes, for example, Complete Active Space with Second-order Perturbation Theory (CASPT2), Equation-Of-Motion Coupled-Cluster Single and Double (EOM-CCSD) and Multi-Reference Configuration Interaction (MR-CI). If one looks for meaningful theory–experiment comparisons, one should compute the 0–0 energies—which can be compared to the absorption/fluorescence crossing point (AFCP)—and/or the band topologies,[3−9] but the two properties necessitate the calculation of ES vibrations, and consequently an efficient access to numerical or analytical second derivatives should be available. Except for tiny molecules, this effectively prevents the use of the three above-mentioned methods, and one has to resort to less refined schemes, for example, CAS-Self Consistent Field (CAS-SCF), Configuration Interaction Singles (CIS), Time-Dependent Density Functional Theory (TD-DFT) and, to some extent, second-order approximate CC (CC2). Among these methods, TD-DFT is clearly the most popular due to (i) its numerous user-friendly implementations; (ii) its ability to provide reasonable estimates of transition energies at a moderate cost; (iii) the ease to combine TD-DFT with environmental models,[10] like the well-known Polarizable Continuum Model

Received: June 28, 2014
Published: August 19, 2014

   dx.doi.org/10.1021/ct500552e | J. Chem. Theory Comput. 2014, 10, 4548–4556

Scheme 1. Representation of the Molecules under Investigation

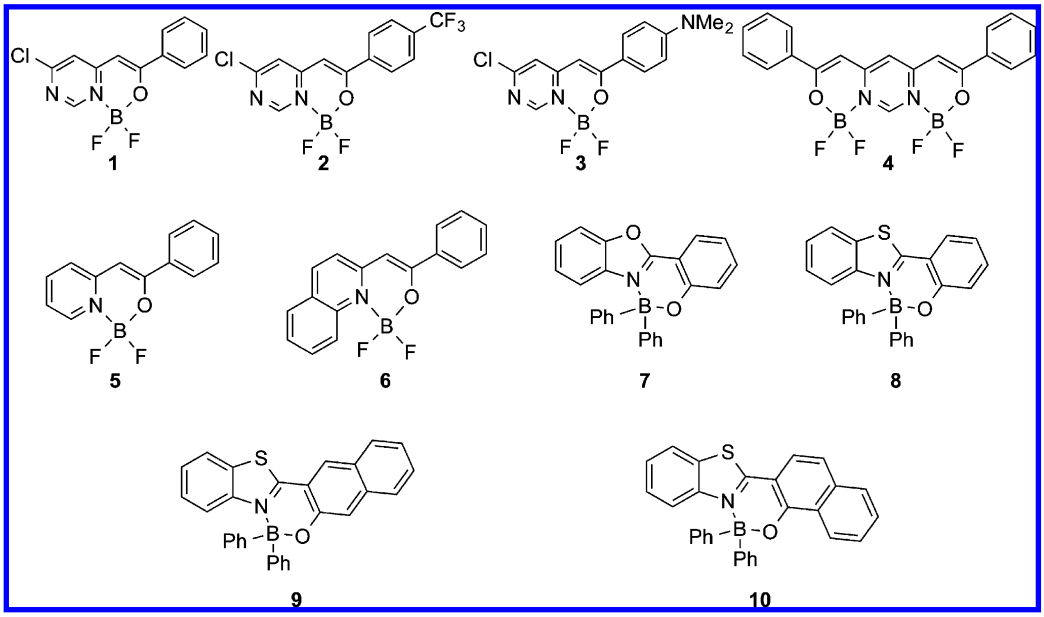

(PCM);[11] and (iv) the availability of both analytic first[3,12,13] and second[14,15] derivatives. No other approach combines these four advantages.

However, standard TD-DFT is not a panacea as it suffers from several significant flaws. For low-lying states of closed-shell molecules, that constitute the majority of relevant cases for practical applications, the main difficulties are encountered with, on the one hand, charge-transfer (CT) ES and, on the other hand, cyanine ES. For the former, standard exchange-correlation functionals (XCF) tend to yield too small transition energies,[16,17] but this problem can be effectively circumvented by using range-separated XCF.[18−20] For the latter, all XCF provide quite similar transition energies[2,21,22] (though the most modern hybrid XCF improve the results),[23−25] that are systematically too large. This is a significant shortcoming as cyanine dyes are one of the most important classes of colored molecules, with several applications in both materials and bioprocess. For example, boron−dipyrromethene (BODIPY) derivatives have become extremely popular.[26−28] In that framework, our groups have recently shown that the Green's function GW and Bethe−Salpeter (BSE) formalisms offer an excellent compromise between computer cost (see below) and accuracy, with a mean absolute error of about 30 meV as compared to exCC3 calculations for the cyanine family.[29] While for the model merocyanine dyes used in all these methodological works,[2,21−25,29] the assessment of TD-DFT calculation accuracy was performed using vertical benchmarks obtained from CAS-PT2, EOM-CC and Diffusion Monte Carlo (DMC) calculations,[22] it was shown that this overshooting trend of TD-DFT pertains to the 0−0 energies of BODIPY and other fluoroborate derivatives that present a central core corresponding to a *cis*-constrained cyanine.[30−33] In particular, boranil dyes, that possess a central nitrogen−boron−oxygen (NBO) atomic sequence (see Scheme 1) apparently concentrate several challenges: besides 0−0 energies that are overshot by most hybrid XCF, solvent effects are both rather large and strongly dependent on the selected solvent model in NBO dyes.[32] Indeed, for boranil and other NBO molecules the results obtained with the linear-response (LR) and state-specific (SS) variations of the PCM vastly differ with several XCF.[32] More puzzling is the fact that the latter more refined SS scheme tends to provide less consistent estimates than the simpler LR approach. At this stage, it is difficult to know if this unexpected outcome is to be mainly attributed to limitations of TD-DFT, of the selected XCF or of the PCM.

In the present work, we tackle the 10 NBO dyes shown in Scheme 1. These molecules have been recently synthesized,[34−36] and no theoretical investigations were performed beyond some calculations of molecular orbitals[36] and purely vertical TD-DFT transition energies.[35] Of course, from the above analysis of literature data, it seems that we have reached a deadlock: the highly correlated wave function models are computationally nontractable for the considered compounds (some have more than 20 conjugated π-electrons), whereas TD-DFT will probably be inaccurate. In addition, the BSE method is, up to now, only available for vertical calculations (no analytical gradients have been obtained yet for BSE)[37] which does not allow a direct access to 0−0 energies, and solvation models are still to be developed. For this reason, we have decided to propose a mixed approach in which the structure and vibrational energies are determined with TD-DFT, but the vertical transition energies are computed with BSE. To the very best of our knowledge, this is the first contribution proposing such combination. However, it is certainly worth pointing out that Grimme et al. proposed a similar blend of models in which they combined CIS(D), configuration interaction singles with perturbative correction for doubles,[38] with TD-DFT to determine 0−0 energies,[4,39] whereas Hattig and co-workers have recently performed a 0−0 benchmark in which, for the largest molecules, TD-DFT vibrational energies are used to correct CC2 adiabatic energies.[7] Nevertheless, these previous works did not focused on cyanine ES, and either considered only the gas phase situation[7,39] or treated solvent effects with the LR-PCM approach.[4]

This paper is organized as follows: in the next section we describe both our computational protocol designed to obtain the AFCP energies directly comparable to experiment and give computational details. In the following section we describe and discuss the main results (influence of auxochromes on the nature of excited states, importance of solvent effects, and

comparisons between BSE and TD-DFT results) before concluding.

METHODS

Protocol. As we used a mixed BSE/TD-DFT procedure in the present work, it is important to accurately define our protocol. For the TD-DFT part, we follow the notation of ref 6, R^{GS} and R^{ES} being the optimal ground and excited-state geometries, respectively, whereas E^{GS} and E^{ES} are the total energies determined for the GS and ES, respectively. First, let us define the vertical absorption and emission energies as the differences between the ES and GS energies determined on the GS and ES optimal structures, respectively.

$$E^{\text{vert}-a} = E^{ES}(R^{GS}) - E^{GS}(R^{GS}) \quad (1)$$

$$E^{\text{vert}-f} = E^{ES}(R^{ES}) - E^{GS}(R^{ES}) \quad (2)$$

Likewise, the reorganization energies can be obtained as the energy changes for a given state following the structural relaxation.

$$E^{\text{reorg}-GS} = E^{GS}(R^{ES}) - E^{GS}(R^{GS}) \quad (3)$$

$$E^{\text{reorg}-ES} = E^{ES}(R^{GS}) - E^{ES}(R^{ES}) \quad (4)$$

The adiabatic energy can be defined in two perfectly equivalent ways:[6]

$$E^{\text{adia}} = E^{ES}(R^{ES}) - E^{GS}(R^{GS}) \quad (5)$$

$$= \frac{1}{2}[E^{\text{vert}-f} + E^{\text{vert}-a}] + \frac{1}{2}[E^{\text{reorg}-GS} - E^{\text{reorg}-ES}] \quad (6)$$

Note that in the latter equation, the first term corresponding to the average of absorption and emission energies strongly dominates the difference of reorganization energies for most dyes. The 0−0 energies are obtained from the adiabatic energies by the simple addition of the vibrational zero-point energies.

$$\Delta E^{ZPVE} = E^{ZPVE}(R^{ES}) - E^{ZPVE}(R^{GS}) \quad (7)$$

$$E^{0-0} = E^{\text{adia}} + \Delta E^{ZPVE} \quad (8)$$

In this work, we included solvent effects through several models derived from the PCM (see below), and this required additional details. In solution, the 0−0 energies become

$$E^{0-0}(X, \text{eq}) = E^{\text{adia}}(X, \text{eq}) + \Delta E^{ZPVE}(\text{LR}, \text{eq}) \quad (9)$$

$$E^{\text{adia}}(X, \text{eq}) = E^{ES}(R^{ES}, X, \text{eq}) - E^{GS}(R^{GS}, \text{PCM}, \text{eq}) \quad (10)$$

$$\Delta E^{ZPVE}(\text{LR}, \text{eq}) = E^{ZPVE}(R^{ES}, \text{LR}, \text{eq}) - E^{ZPVE}(R^{GS}, \text{PCM}, \text{eq}) \quad (11)$$

where X denotes the solvent model: LR, corrected LR (cLR), or SS in our case, and eq indicates that the equilibrium solvation limit is applied (see next Section). In eqs 10 and 11, we put X = PCM for ground-state properties since, in that case all solvation models are equivalent. We underline that analytic TD-DFT gradients are only available with the LR model, so that both the geometries and ZPVE energies are systematically determined with the LR-PCM approach, cLR and SS terms being included as energy corrections. To obtain the AFCP energies we should add a correction for nonequilibrium effects (neq), as both absorption and emission are better described in the nonequilibrium PCM limit (see next Section):

$$E^{\text{AFCP}}(X, \text{neq}) = E^{0-0}(X, \text{eq}) + \frac{1}{2}[\Delta E^{\text{vert}-a}(X) + \Delta E^{\text{vert}-f}(X)] \quad (12)$$

$$\Delta E^{\text{vert}-a}(X) = E^{\text{vert}-a}(X, \text{neq}) - E^{\text{vert}-a}(X, \text{eq}) \quad (13)$$

$$= E^{ES}(R^{GS}, X, \text{neq}) - E^{ES}(R^{GS}, X, \text{eq}) \quad (14)$$

$$\Delta E^{\text{vert}-f}(X) = E^{\text{vert}-f}(X, \text{neq}) - E^{\text{vert}-f}(X, \text{eq}) \quad (15)$$

$$= E^{GS}(R^{ES}, \text{PCM}, \text{eq}) - E^{GS}(R^{ES}, X, \text{neq}) \quad (16)$$

and this completely defines our approach for the PCM-TD-DFT part of the calculation. Extensive benchmarks with this approach and X = cLR can be found elsewhere.[6]

With BSE, we have access to the gas-phase vertical transition energies, $E_{BSE}^{\text{vert}-a}$ and $E_{BSE}^{\text{vert}-f}$. Starting from eq 5, it is therefore straightforward to obtain the adiabatic BSE energy as

$$E_{BSE}^{\text{adia}} = \frac{1}{2}[E_{BSE}^{\text{vert}-f} + E_{BSE}^{\text{vert}-a}] + \frac{1}{2}[E_{TD-DFT}^{\text{reorg}-GS} - E_{TD-DFT}^{\text{reorg}-ES}] \quad (17)$$

to which further corrections for the solvent effects can be added, by using the solvatochromic shifts provided by the PCM-TD-DFT approaches.

$$E_{BSE}^{\text{adia}}(X, \text{eq}) = E_{BSE}^{\text{adia}} + [E_{TD-DFT}^{\text{adia}}(X, \text{eq}) - E_{TD-DFT}^{\text{adia}}] \quad (18)$$

which defines a best estimate for the BSE adiabatic energies in solution. At this point, one just needs to insert eq 18 in eqs 9 and 12 to reach the AFCP energies using vertical BSE transition energies and solvent/vibrational data originating from TD-DFT:

$$E_{BSE}^{\text{AFCP}}(X, \text{neq}) = E_{BSE}^{\text{adia}}(X, \text{eq}) + \Delta E_{TD-DFT}^{ZPVE}(\text{LR}, \text{eq}) + \frac{1}{2}[\Delta E_{TD-DFT}^{\text{vert}-a}(X) + \Delta E_{TD-DFT}^{\text{vert}-f}(X)] \quad (19)$$

$$= E_{BSE}^{0-0}(X, \text{eq}) + \frac{1}{2}[\Delta E_{TD-DFT}^{\text{vert}-a}(X) + \Delta E_{TD-DFT}^{\text{vert}-f}(X)] \quad (20)$$

The present contribution provides an extensive comparison of the merits of the pure TD-DFT approach, eq 12, and the mixed model, eq 19, for the series of compounds shown in Scheme 1.

The GW-BSE Approach. The many-body Green's function GW and Bethe−Salpeter calculations proceed in two steps. One starts first with a GW calculation[40−46] that aims at providing accurate quasiparticle energies, namely both occupied and virtual energy levels, including in particular the highest occupied molecular orbital (HOMO) and lowest unoccupied molecular orbital (LUMO) energy levels. The eigenvalue equation reads:

$$\left(\frac{-\nabla^2}{2} + V^{\text{ionic}}(\mathbf{r}) + V^{\text{Hartree}}(\mathbf{r})\right)\phi(\mathbf{r}) + \int d\mathbf{r}'\Sigma(\mathbf{r}, \mathbf{r}'; E)\phi(\mathbf{r}') = E\phi(\mathbf{r}) \quad (21)$$

where the nonlocal and energy-dependent self-energy operator Σ accounts for exchange and correlation. Within Schwinger's

dx.doi.org/10.1021/ct500552e | J. Chem. Theory Comput. 2014, 10, 4548−4556

functional derivative approach to perturbation theory,[47] the GW approximation to the self-energy reads:

$$\Sigma^{\mathrm{GW}}(\mathbf{r}, \mathbf{r}'; E) = \frac{i}{2\pi}\int \mathrm{d}\omega \mathrm{e}^{-i\delta\omega} G(\mathbf{r}, \mathbf{r}'; E+\omega) W(\mathbf{r}, \mathbf{r}'; \omega) \tag{22}$$

where $G(\mathbf{r}, \mathbf{r}'; E)$ and $W(\mathbf{r}, \mathbf{r}'; \omega)$ are the one-particle time-ordered Green's function and dynamically screened Coulomb potential, namely,

$$G(\mathbf{r}, \mathbf{r}'; E+\omega) = \sum_n \frac{\phi_n(\mathbf{r})\phi_n^*(\mathbf{r}')}{E+\omega-\varepsilon_n - i\delta \mathrm{sgn}(\varepsilon_n - \mu)} \tag{23}$$

$$\chi_0(\mathbf{r}, \mathbf{r}'; \omega) = \sum_{n,n'} \frac{f_n - f_{n'}}{\varepsilon_n - \varepsilon_{n'} - \omega} \phi_n^*(\mathbf{r})\phi_{n'}(\mathbf{r})\phi_{n'}^*(\mathbf{r}')\phi_n(\mathbf{r}') \tag{24}$$

$$W(\mathbf{r}, \mathbf{r}'; \omega) = v(\mathbf{r}, \mathbf{r}') + \int\int \mathrm{d}\mathbf{r}_1 \mathrm{d}\mathbf{r}_2 v(\mathbf{r}, \mathbf{r}_1)\chi_0(\mathbf{r}_1, \mathbf{r}_2|\omega) W(\mathbf{r}_2, \mathbf{r}'|\omega) \tag{25}$$

where we introduced the independent-electron susceptibility χ_0. The "input" $\{\varepsilon_n, \phi_n\}$ eigenstates are traditionaly taken to be DFT Kohn−Sham eigenstates. The corrected quasiparticle energies $\{\varepsilon_n^{\mathrm{QP}}\}$ are obtained by replacing the DFT exchange-correlation contribution to the DFT eigenvalues, namely:

$$\varepsilon_n^{\mathrm{QP}} = \varepsilon_n^{\mathrm{DFT}} + \langle \phi_n | \Sigma^{\mathrm{GW}}(\mathbf{r}, \mathbf{r}'; \varepsilon_n^{\mathrm{QP}}) - V^{xc} | \phi_n \rangle \tag{26}$$

Once the quasiparticle energy spectrum is determined, the optical absorption spectrum can be tackled within the BSE formalism[48−54] that introduces the electron−hole interaction. The optical excitation energies are eigenstates of the BSE Hamiltonian expressed in the product space of the occupied and virtual single-particle states, namely:

$$\begin{pmatrix} R & C \\ -C^* & -R^* \end{pmatrix} \cdot \begin{pmatrix} [\phi_a(\mathbf{r}_e)\phi_i(\mathbf{r}_h)] \\ [\phi_i(\mathbf{r}_e)\phi_a(\mathbf{r}_h)] \end{pmatrix} = \Omega^{\mathrm{BSE}} \begin{pmatrix} [\phi_a(\mathbf{r}_e)\phi_i(\mathbf{r}_h)] \\ [\phi_i(\mathbf{r}_e)\phi_a(\mathbf{r}_h)] \end{pmatrix} \tag{27}$$

where the indexes (i,j) and (a,b) here and below indicate the occupied and virtual orbitals, and $(\mathbf{r}_e, \mathbf{r}_h)$ the electron and hole positions, respectively. Ω^{BSE} are the BSE excitation energies. The resonant contribution (R) reads:

$$R_{ai,bj} = \delta_{a,b}\delta_{i,j}(\varepsilon_a^{\mathrm{QP}} - \varepsilon_i^{\mathrm{QP}}) - \iint \phi_a(\mathbf{r}_e)\phi_i(\mathbf{r}_h) W(\mathbf{r}_e, \mathbf{r}_h)\phi_b(\mathbf{r}_e)\phi_j(\mathbf{r}_h)\mathrm{d}\mathbf{r}_h\mathrm{d}\mathbf{r}_e + 2\eta \iint \phi_a(\mathbf{r}_e)\phi_i(\mathbf{r}_e) V^C(\mathbf{r}_e, \mathbf{r}_h)\phi_b(\mathbf{r}_h)\phi_j(\mathbf{r}_h)\mathrm{d}\mathbf{r}_h\mathrm{d}\mathbf{r}_e \tag{28}$$

with $\eta = 1$ for the singlet states studied here. We go beyond the Tamm−Dancoff approximation by mixing resonant and nonresonant excitations as described by the off-diagonal (C) block. Such a formulation resembles the TD-DFT equations within Casida's formulation[55] and offers consequently the very same computational cost and scaling once the screened Coulomb potential W has been calculated. Besides the case of the cyanines,[29] the success of the Bethe−Salpeter formalism for the description, for example, of Frenkel and charge-transfer excitations in gas phase organic systems has been recently emphasized by several groups.[56−65]

Computational Details. All DFT and TD-DFT computations have been performed with the Gaussian09 program package,[66] applying default thresholds except for a tighten self-consistent field convergence (10^{-8}−10^{-10} a.u.), an improved optimization threshold (10^{-5} a.u. on average forces) and an enhanced DFT integration grid (*ultrafine* grid). For each molecule, we have optimized the geometry of both the ground and the first excited states, as well as computed the vibrational spectra of both states. For all DFT and TD-DFT calculations, we have applied the M06-2X global hybrid *meta*-GGA exchange-correlation functional that includes 54% of *exact* exchange.[67] This choice is justified by numerous benchmarks that have shown that M06-2X is one of the most-suited approaches to investigate the excited-state energies and structures of many classes of molecules,[2,6,67−71] and this general statement holds for cyanine, BODIPY and NBO derivatives as well.[24,31,32] In a recent work, we have assessed basis set effects for aza-BODIPY dyes.[30] It was found that the geometrical and vibrational parameters can be determined with a relatively compact atomic basis set, that is 6-31G(d), whereas the transition energies need to be corrected using a more extended atomic basis set, namely 6-311+G(2d,p). Consequently, we have used the former (latter) basis set to obtain the optimal structures and ZPVE energies (total and transition energies). The same 6-311+G(2d,p) atomic basis set is used for the BSE calculations (see below).

The inclusion of environmental effects is often crucial to estimate the electronic transition energies, and solvation effects (here dichloromethane for **1**−**6** and toluene for **7**−**10**, consistently with experiments)[34−36] have been quantified using the PCM approach.[11] We have applied the LR scheme[72,73] for geometry optimizations and calculations of the vibrational frequencies, whereas the total and transition energies have been tackled with three approaches: LR,[72,73] cLR,[74] and SS models.[75] In all cases, the solvent polarization is represented in terms of induced charges on the surface of a cavity embedding the molecule, however the way this polarization changes from the ground to the excited state differs. In the LR scheme, the transition densities are used to determine the changes of the PCM charges. In the cLR scheme, the one-particle TD-DFT density matrix, that accounts for the orbital relaxation contribution, is used in a perturbative approach. In the SS scheme, a self-consistent formulation is used, but at the price of a modification of the ground-state reference. For all three PCM variations, two light-matter interactions limits can be defined: the equilibrium and nonequilibrium schemes. In the neq limit, only the electrons of the solvent adapt to the new electronic configuration of the solute (fast process). Clearly, the absorption and emission energies better correspond to a neq scheme. On the contrary, in the eq approach, the solvent molecular structure has also time to adapt to the new electronic configuration of the solute (slow process). This latter approach is the recommended approach to calculate excited-state geometries, vibrational signatures and consequently adiabatic energies.

The BSE calculations are performed with the Fiesta package,[61,76,77] a Gaussian-basis implementation of the GW and Bethe-Salpeter formalisms using the resolution-of-the-identity approach with the Coulomb metric.[78] Within such an approach, GW calculations offer a N^4 scaling and are amenable to systems comprising a few hundred atoms.[65] Namely, in our case, the GW calculation (six partial self-consistent iterations) for one molecule takes roughly 4 h of walltime on eight cores (Intel E5−2680 [Sandy-Bridge EP] with 2.7 GHz peak frequency per core), while the BSE part only takes 38 min on 16 cores. Dynamical correlations are calculated within an exact contour deformation technique, avoiding namely any plasmon-pole approximation. Our starting DFT eigenstates are

dx.doi.org/10.1021/ct500552e | J. Chem. Theory Comput. 2014, 10, 4548−4556

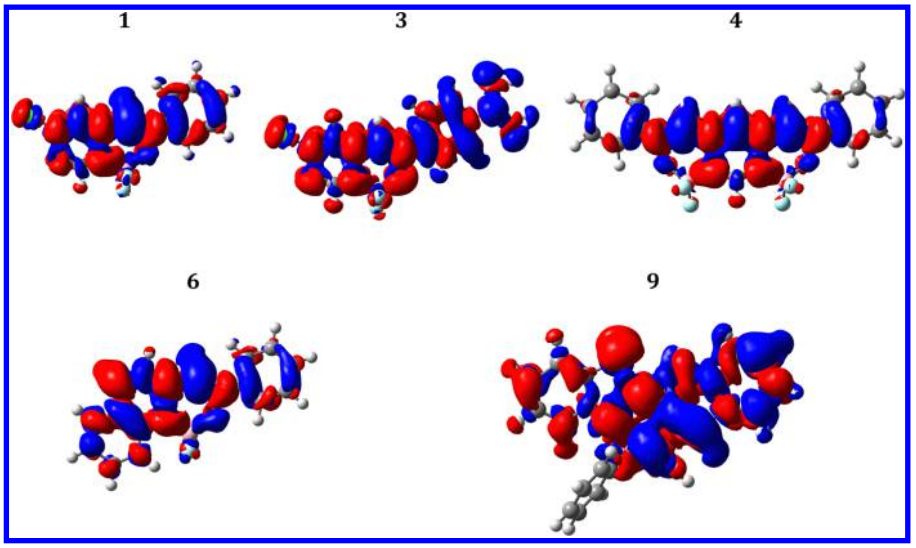

Figure 1. Density difference plots for five selected compounds. The blue (red) regions correspond to decrease (increase) of the electron density upon photon absorption. The used contour threshold is 0.0004 au in all cases.

Table 1. TD-DFT and Experimental Energies for the 0−0/AFCP Energies Using a Panel of Solvation Models[a]

	E^{0-0}[b]				E^{AFCP}[c]		
dye	gas	X = LR	X = cLR	X = SS	X = cLR	X = SS	exp
1	3.588	3.272	3.547	3.510	3.557	3.556	3.094
2	3.581	3.292	3.552	3.523	3.558	3.549	3.121
3	3.304	2.829	3.084	2.922	3.122	3.087	2.522
4	3.126	2.780	3.060	3.004	3.063	3.020	2.570
5	3.494	3.246	3.507	3.502	3.517	3.569	2.939
6	3.238	3.013	3.244	3.246	3.251	3.282	2.786
7	3.305	3.291	3.331	3.353	3.331	3.354	3.019
8	3.108	3.103	3.137	3.157	3.137	3.160	2.861
9	2.755	2.795	2.769	2.754	2.769	2.761	2.459
10	2.975	2.933	2.983	2.991	2.984	2.991	2.723
MSE	0.438	0.246	0.412	0.387	0.420	0.424	
MAE	0.438	0.246	0.412	0.387	0.420	0.424	
R^2	0.604	0.949	0.810	0.898	0.783	0.809	

[a]At the bottom of the Table, statistical data are listed. All data (but R^2) are in eV. The experimental data have been deduced from refs 34−36. [b]The equilibrium E^{0-0} values are derived from eq 9. [c]The non-equilibrium E^{AFCP} values are derived from eq 12.

calculated with the NWChem package[79] using the very same 6-311+G(2d,p) basis as the one used for the TD-DFT calculations. Our auxiliary basis is the universal auxiliary basis developed in ref 80. This computational scheme is rigorously similar to that adopted in the recent study of the cyanine family where close agreement with exCC3 calculations was demonstrated for vertical absorption energies.[29] While all virtual states are used to build the independent-electron susceptibility, inclusion of 460 virtual states are used at convergence for building the Bethe-Salpeter Hamiltonian (see Supporting Information for convergence tests on molecule **2**).

Following the study of cyanines in ref 29, we adopt a self-consistent GW approach that avoids any starting point dependence, namely any variation of the final quasiparticle energies with the exchange-correlation functional used to build the input DFT Kohn−Sham eigenstates. The calculated G and W operators are build self-consistently by reinjecting the calculated quasiparticle eigenstates. We perform self-consistency on the wave functions at the "static" GW level within the so-called Coulomb-hole plus screened-Exchange (COHSEX) approximation to the self-energy, a self-consistent scheme widely used in the study of extended semiconductors.[81] Such an approach was shown to provide the best results for the cyanine family, even though nonself-consistent approaches, namely, keeping input PBE or Hartree−Fock wave functions frozen, while updating the quasiparticle eigenvalues only, would lead to errors within 0.15 eV as compared to exCC3 calculations, which is overall a better agreement with exCC3 calculations as compared to available TD-DFT calculations with semilocal, global or range-separated hybrid functionals. We underline that the gas-phase TD-DFT and BSE transition energies used in eqs 17 and 18 have been obtained through "single-point" calculations on the GS and ES structures optimized with PCM.

RESULTS AND DISCUSSION

Nature of the Excited States. We have first assessed the topology of the electronic excited-states using both density difference plots that allow to represent an electronic transition with a single picture, and Le Bahers' model that quantifies the CT nature of the ES.[82,83] For the former, the results can be found in Figure 1. For most structures, at the notable exception of **3** that bears a dialkylamino side group, we found clearly

dx.doi.org/10.1021/ct500552e | J. Chem. Theory Comput. 2014, 10, 4548−4556

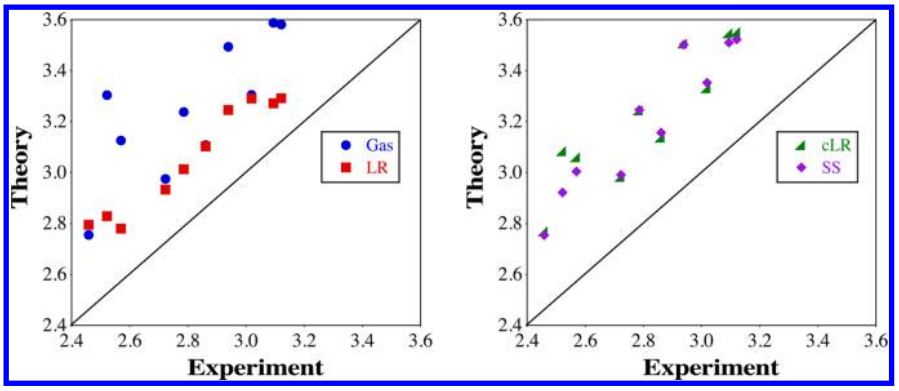

Figure 2. Comparison between experimental and TD-DFT 0−0 energies (in eV), using different environmental models in their equilibrium limits. The central diagonal indicates a perfect experiment−theory match.

Table 2. BSE, eq 19, and Experimental Energies for the 0−0/AFCP Energies Using a Panel of Solvation Models[a]

	E^{0-0}				E^{AFCP}		
dye	gas	X = LR	X = cLR	X = SS	X = cLR	X = SS	exp
1	3.358	3.042	3.317	3.280	3.327	3.326	3.094
2	3.282	2.993	3.253	3.224	3.260	3.250	3.121
3	3.090	2.614	2.870	2.708	2.908	2.872	2.522
4	2.880	2.534	2.814	2.758	2.817	2.774	2.570
5	3.108	2.860	3.121	3.116	3.131	3.184	2.939
6	2.919	2.695	2.925	2.927	2.933	2.964	2.786
7	2.971	2.957	2.997	3.018	2.997	3.020	3.019
8	2.866	2.860	2.895	2.915	2.895	2.918	2.861
9	2.361	2.401	2.376	2.360	2.376	2.368	2.459
10	2.697	2.654	2.705	2.713	2.706	2.712	2.723
MSE	0.144	−0.048	0.118	0.093	0.125	0.129	
MAE	0.178	0.067	0.143	0.115	0.150	0.150	
R^2	0.520	0.944	0.747	0.871	0.718	0.765	

[a]See caption of Table 1 for more details.

alternating regions of electron density gain and loss, which is typical of cyanine-like states. This is especially clear for the highly symmetric **4** that presents an ES visually very similar to the one found in canonical merocyanines.[84] For **1**, **6**, and **9**, the ES is slightly more asymmetric, but Le Bahers' model provides CT distances of 1.60, 1.37, and 1.86 Å, respectively, rather small values.[82,83] For **9**, we notice nevertheless a small CT character, the benzothiazole moiety acting like an electron acceptor. For **3**, on the contrary, a much stronger CT (distance of 3.35 Å) is obtained, the amino group being a donor (mostly in blue in Figure 1), as could be expected. In short, this confirms that all the considered dyes but **3** can be viewed as presenting a delocalized ES with moderate CT.

Solvent Effects with TD-DFT. We compare experimental and TD-DFT transition energies in Table 1 and Figure 2. As expected (see Introduction) TD-DFT systematically yields too large values, irrespective of the molecule considered or the selected environmental model. We also note that the selection of the equilibrium (E^{0-0}) or the nonequilibrium (E^{AFCP}) limit induces trifling (cLR) or very small (SS) differences for most dyes, the only exception being **3**, the compound presenting the strongest CT signature and hence the largest change of dipole moment between the GS and the ES (+8.87 D in **3** to be compared to +2.19 D in **1**). For **7**−**10**, measured in the apolar toluene, all variations of the PCM model provide solvatochromic shifts smaller than 0.05 eV. For **1**−**6** studied in the more polar dichloromethane, the LR E^{0-0} are significantly smaller than their gas phase counterparts, whereas gas, cLR, and SS values remain rather close, the only exception to this general trend being, again, **3**. In other words, LR provides a much stronger solvatochromic effect than both cLR and SS for cyanine-like dyes, a fact already observed in both NBO and dioxoborine dyes.[32,33]

At the bottom of Table 1, we list the mean signed error (MSE), mean absolute error (MAE) and determination coefficient obtained through linear least-squares fitting (R^2). The poorest results are obtained with the gas-phase approach that yields the largest MAE and, by far, the smallest R^2. This small R^2 is significantly enhanced (from 0.604 to 0.801) when removing **3** from the series. This illustrates that the lack of modeling of environmental effects is especially detrimental for CT ES. As expected from the above analysis, adding the nonequilibrium correction either does not modify (cLR) or slightly deteriorates (SS) the statistical data obtained in the equilibrium limit. One clearly notices that the LR scheme not only provides the smallest MAE but also delivers the best consistency with experiments: it is the only method that gives a MAE below 0.3 eV and an R^2 exceeding the 90% mark. This nice correlation is obvious from the left panel of Figure 2. The slope of the correlation line is also closer to unity for LR than for cLR or SS. As we previously discussed,[33] such results raises a dilemma since the more advanced solvation models (cLR and SS) apparently yield poorer results than the simplest approach (LR). Of course this success of LR might originate in an error

dx.doi.org/10.1021/ct500552e | J. Chem. Theory Comput. 2014, 10, 4548−4556

compensation between the TD-DFT overshooting of the transition energies for cyanine ES and the LR-PCM overestimation of the stabilization energies for most dyes.[6]

Impact of BSE Corrections. The results obtained by accounting for BSE corrections are collected in Table 2. One clearly notices that BSE improves the results compared to TD-DFT: the theoretical transition energies reported in Table 2 are systematically closer to experiment than the one listed in Table 1. Another striking fact is that the MSE and MAE are no more equal, indicating that there is no more significant overshooting of the experimental values. The MSE and MAE are now systematically smaller than 0.2 eV, irrespective of the selected environmental approach. In that sense BSE brings a very significant improvement to the raw TD-DFT results. On the other hand, the R^2 computed with the BSE correction are smaller than their TD-DFT counterparts, though the changes are not significant for the LR and SS models. LR-PCM still provides the most accurate results when BSE corrections are accounted for, and the good match with experiment is obvious from Figure 3.

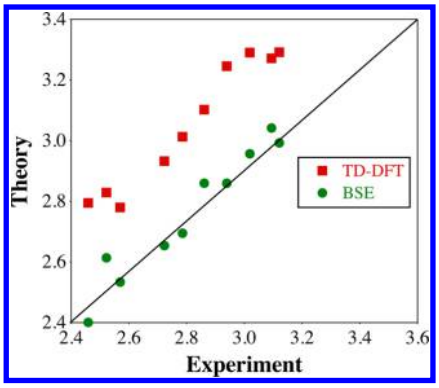

Figure 3. Comparisons between experimental, TD-DFT and BSE energies considering the LR,eq PCM approach. All data are in eV.

To determine if the improvements brought by the vertical BSE calculations can be mostly ascribed to the vertical absorption or the corresponding emission, we have investigated the differences between the TD-DFT and BSE gas-phase transitions computed on the ground and excited-state geometries. For absorption, the BSE correction ranges from −0.127 eV (**3**) to −0.423 eV (**9**) with an average value of −0.271 eV. For emission, the BSE decreases the TD-DFT values by an average of −0.317 eV with minimal and maximal changes of −0.230 eV (**1**) and −0.405 eV (**5**), respectively. One can conclude that the BSE corrections tend to be larger for the more conjugated excited-state geometries, though this trend is not systematic.

To conclude this discussion, we provide in Figure 4 a plot of the (TD-)DFT GS and ES energies along the pathway connecting the optimal GS and ES geometries for molecule **5**. We focus on gas phase calculations to set aside issues related to solvation models. The selected geometries are inter/extrapolated from the related two optimal geometries. We further plot an *ansatz* BSE energy surface by adding the BSE excitation energy to the ground-state DFT energy. Since GS/ES geometry optimization are not available within the GW-BSE formalism, at least for rather large systems,[85] monitoring the GW or BSE excited-state energies along a DFT, constrained-DFT or TD-DFT relaxation pathway offers a minimal test to

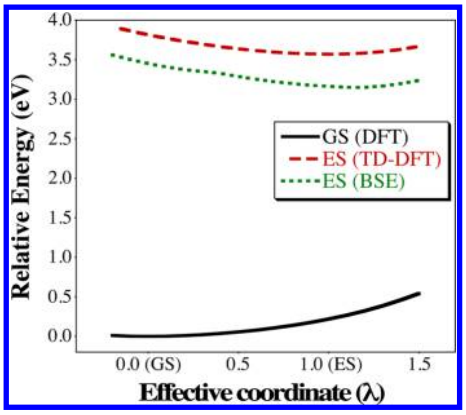

Figure 4. DFT GS (full black line) and TD-DFT lowest singlet ES (dashed red line) energies along the effective coordinate connecting the DFT ground-state relaxed geometry (λ = 0) and TD-DFT excited-state relaxed geometry (λ = 1) for molecule **5**. All calculations are performed in gas phase using the 6-311+G(2d,p) atomic basis set for both the optimization of the geometries and the determination of the transition energies. Configurations have been interpolated and extrapolated along that configurational pathway. The BSE excited-state energy line (dotted green line) is represented as the sum of the DFT ground-state energy plus the BSE transition energy. A quadratic fit around the Bethe−Salpeter excited state minimum has been used to estimate the BSE minimum energy and its 16 meV difference with the BSE energy at the TD-DFT excited-state relaxed structure.

verify that the BSE ES minimum in configuration space is not too distant from the value calculated at the DFT relaxed geometry.[37,86−89] This is what we observe in the present case where the minimum BSE energy is obtained close to the TD-DFT minimum, with a marginal 16 meV difference between the BSE excited state energy at the TD-DFT relaxed structure and the minimum BSE energy along this specific pathway. Besides the very clear improvement when compared to experiment, the present test further validates the proposed TD-DFT/BSE hybrid scheme by demonstrating that the vertical BSE correction is, by far, dominant.

CONCLUSIONS AND OUTLOOK

We have investigated the transition energies of ten recently synthesized NBO dyes with a refined approach relying on TD-DFT to obtain geometries, vibrational signatures and solvatochromic shifts, and using BSE to determine vertical transition energies. This blend of approaches undoubtedly allows to improve the theoretical estimates compared to "pure" TD-DFT results that are systematically too large compared to the experimental references. Indeed, the BSE correction significantly decreases the mean absolute deviation compared to experiment (from 0.25−0.45 eV with TD-DFT to 0.07−0.18 eV with BSE), though it does not improve the quality of the chemical trends (R^2). In addition, we have investigated solvent effects using a panel of declinations of the PCM approach, and we found that (i) the nonequilibrium corrections are either trifling (cLR) or negligible (SS); (ii) LR provides larger solvatochromic corrections and a better consistency with experimental trends; (iii) cLR and SS values are often very similar but for ES with a strong CT character.

While this study provides a practical way to improve TD-DFT estimates for challenging dyes thanks to the addition of a BSE correction, it remains that both the structures and solvent effects have been estimated using an approach that does not appear ideal for cyanine ES. In that framework, BSE geometry

dx.doi.org/10.1021/ct500552e | J. Chem. Theory Comput. 2014, 10, 4548−4556

optimizations and estimations of solvent shifts would clearly be welcome. Both are, to the best of our knowledge, not yet available, but we are currently working in these directions.

■ ASSOCIATED CONTENT

Supporting Information

Convergence of BSE calculations. Cartesian coordinates of the ground and excited-state structures. This material is available free of charge via the Internet at http://pubs.acs.org/.

■ AUTHOR INFORMATION

Corresponding Authors

*E-mail: xavier.blase@neel.cnrs.fr.

*E-mail: Denis.Jacquemin@univ-nantes.fr.

Author Contributions

#Contributed equally to this work.

Notes

The authors declare no competing financial interest.

■ ACKNOWLEDGMENTS

D.J. is indebted to K.J. Chen for her kind help. P.B. acknowledges postdoctoral funding from the French ANR program under Contract No. ANR-2012-BS04 PANELS. S.C. acknowledges the European Research Council (ERC) for financial support of her Ph.D. grant under the Marches (278845) program. D.J. acknowledges the ERC and the *Région des Pays de la Loire* for financial support in the framework of a Starting Grant (Marches 278845) and a *recrutement sur poste stratégique*, respectively. This research used resources of (1) the GENCI-CINES/IDRIS (Grant No. c2013085117), (2) *Centre de Calcul Intensif des Pays de Loire* (CCIPL); and (3) a local Troy cluster.

■ REFERENCES

(1) Laurent, A. D.; Adamo, C.; Jacquemin, D. *Phys. Chem. Chem. Phys.* **2014**, *16*, 14334−14356.

(2) Laurent, A. D.; Jacquemin, D. *Int. J. Quantum Chem.* **2013**, *113*, 2019−2039.

(3) Furche, F.; Ahlrichs, R. *J. Chem. Phys.* **2002**, *117*, 7433−7447.

(4) Goerigk, L.; Grimme, S. *J. Chem. Phys.* **2010**, *132*, 184103.

(5) Send, R.; Kühn, M.; Furche, F. *J. Chem. Theory Comput.* **2011**, *7*, 2376−2386.

(6) Jacquemin, D.; Planchat, A.; Adamo, C.; Mennucci, B. *J. Chem. Theory Comput.* **2012**, *8*, 2359−2372.

(7) Winter, N. O. C.; Graf, N. K.; Leutwyler, S.; Hattig, C. *Phys. Chem. Chem. Phys.* **2013**, *15*, 6623−6630.

(8) Avila Ferrer, F. J.; Cerezo, J.; Stendardo, E.; Improta, R.; Santoro, F. *J. Chem. Theory Comput.* **2013**, *9*, 2072−2082.

(9) Fang, C.; Oruganti, B.; Durbeej, B. *J. Phys. Chem. A* **2014**, *118*, 4157−4171.

(10) Jacquemin, D.; Mennucci, B.; Adamo, C. *Phys. Chem. Chem. Phys.* **2011**, *13*, 16987−16998.

(11) Tomasi, J.; Mennucci, B.; Cammi, R. *Chem. Rev.* **2005**, *105*, 2999−3094.

(12) van Caillie, C.; Amos, R. D. *Chem. Phys. Lett.* **1999**, *308*, 249−255.

(13) Scalmani, G.; Frisch, M. J.; Mennucci, B.; Tomasi, J.; Cammi, R.; Barone, V. *J. Chem. Phys.* **2006**, *124*, 094107.

(14) Liu, J.; Liang, W. Z. *J. Chem. Phys.* **2011**, *135*, 014113.

(15) Liu, J.; Liang, W. Z. *J. Chem. Phys.* **2011**, *135*, 184111.

(16) Tozer, D. J. *J. Chem. Phys.* **2003**, *119*, 12697−12699.

(17) Dreuw, A.; Head-Gordon, M. *J. Am. Chem. Soc.* **2004**, *126*, 4007−4016.

(18) Tawada, T.; Tsuneda, T.; Yanagisawa, S.; Yanai, T.; Hirao, K. *J. Chem. Phys.* **2004**, *120*, 8425−8433.

(19) Rudberg, E.; Salek, P.; Helgaker, T.; Agren, H. *J. Chem. Phys.* **2005**, *123*, 184108.

(20) Lange, A. W.; Rohrdanz, M. A.; Herbert, J. M. *J. Phys. Chem. B* **2008**, *112*, 6304−6308.

(21) Jacquemin, D.; Perpète, E. A.; Scalmani, G.; Frisch, M. J.; Kobayashi, R.; Adamo, C. *J. Chem. Phys.* **2007**, *126*, 144105.

(22) Send, R.; Valsson, O.; Filippi, C. *J. Chem. Theory Comput.* **2011**, *7*, 444−455.

(23) Grimme, S.; Neese, F. *J. Chem. Phys.* **2007**, *127*, 154116.

(24) Jacquemin, D.; Zhao, Y.; Valero, R.; Adamo, C.; Ciofini, I.; Truhlar, D. G. *J. Chem. Theory Comput.* **2012**, *8*, 1255−1259.

(25) Moore, B., II; Autschbach, J. *J. Chem. Theory Comput.* **2013**, *9*, 4991−5003.

(26) Loudet, A.; Burgess, K. *Chem. Rev.* **2007**, *107*, 4891−4932.

(27) Ulrich, G.; Ziessel, R.; Harriman, A. *Angew. Chem., Int. Ed.* **2008**, *47*, 1184−1201.

(28) Frath, D.; Massue, J.; Ulrich, G.; Ziessel, R. *Angew. Chem., Int. Ed.* **2014**, *53*, 2290−2310.

(29) Boulanger, P.; Jacquemin, D.; Duchemin, I.; Blase, X. *J. Chem. Theory Comput.* **2014**, *10*, 1212−1218.

(30) Chibani, S.; Le Guennic, B.; Charaf-Eddin, A.; Maury, O.; Andraud, C.; Jacquemin, D. *J. Chem. Theory Comput.* **2012**, *8*, 3303−3313.

(31) Chibani, S.; Le Guennic, B.; Charaf-Eddin, A.; Laurent, A. D.; Jacquemin, D. *Chem. Sci.* **2013**, *4*, 1950−1963.

(32) Chibani, S.; Charaf-Eddin, A.; Le Guennic, B.; Jacquemin, D. *J. Chem. Theory Comput.* **2013**, *9*, 3127−3135.

(33) Chibani, S.; Charaf-Eddin, A.; Mennucci, B.; Le Guennic, B.; Jacquemin, D. *J. Chem. Theory Comput.* **2014**, *10*, 805−815.

(34) Graser, M.; Kopacka, H.; Wurst, K.; Ruetz, M.; Kreutz, C. R.; Müller, T.; Hirtenlehner, C.; Monkowius, U.; Knör, G.; Bildstein, B. *Inorg. Chim. Acta* **2013**, *405*, 116−120.

(35) Kiprof, P.; Carlson, J. C.; Anderson, D. R.; Nemykin, V. N. *Dalton Trans.* **2013**, *42*, 15120−15132.

(36) Kubota, Y.; Ozaki, Y.; Funabiki, K.; Matsui, M. *J. Org. Chem.* **2013**, *78*, 7058−7067.

(37) Ismail-Beigi, S.; Louie, S. G. *Phys. Rev. Lett.* **2003**, *90*, 076401.

(38) Head-Gordon, M.; Maurice, D.; Oumi, M. *Chem. Phys. Lett.* **1995**, *246*, 114−121.

(39) Grimme, S.; Izgorodina, E. I. *Chem. Phys.* **2004**, *305*, 223−230.

(40) Hedin, L. *Phys. Rev. A* **1965**, *139*, 796−823.

(41) Strinati, G.; Mattausch, H.; Hanke, W. *Phys. Rev. Lett.* **1980**, *45*, 290−294.

(42) Strinati, G.; Mattausch, H.; Hanke, W. *Phys. Rev. B* **1982**, *25*, 2867−2888.

(43) Hybertsen, M. S.; Louie, S. G. *Phys. Rev. B* **1986**, *34*, 5390−5413.

(44) Godby, R. W.; Schlüter, M.; Sham, L. J. *Phys. Rev. B* **1988**, *37*, 10159−10175.

(45) Aryasetiawan, F.; Gunnarsson, O. *Rep. Prog. Phys.* **1998**, *61*, 237.

(46) Aulbur, W. G.; Jönsson, L.; Wilkins, J. W. In *Solid State Physics;* Ehrenreich, H., Spaepen, F., Eds.; Academic Press: Waltham, MA, 1999; Vol. *54*, pp 1−218.

(47) Martin, P. C.; Schwinger, J. *Phys. Rev.* **1959**, *115*, 1342−1373.

(48) Sham, L. J.; Rice, T. M. *Phys. Rev.* **1966**, *144*, 708−714.

(49) Hanke, W.; Sham, L. J. *Phys. Rev. Lett.* **1979**, *43*, 387−390.

(50) Strinati, G. *Phys. Rev. Lett.* **1982**, *49*, 1519−1522.

(51) Strinati, G. *Riv. Nuovo Cimento Soc. Ital. Fis.* **1988**, *11*, 1−86.

(52) Rohlfing, M.; Louie, S. G. *Phys. Rev. Lett.* **1998**, *80*, 3320−3323.

(53) Benedict, L. X.; Shirley, E. L.; Bohn, R. B. *Phys. Rev. Lett.* **1998**, *80*, 4514−4517.

(54) Albrecht, S.; Reining, L.; Del Sole, R.; Onida, G. *Phys. Rev. Lett.* **1998**, *80*, 4510−4513.

(55) Casida, M. E. In *Time-Dependent Density-Functional Response Theory for Molecules;* Chong, D. P., Ed.; Recent Advances in Density Functional Methods; World Scientific: Singapore, 1995; Vol. *1*, pp 155−192.

(56) Tiago, M. L.; Chelikowsky, J. R. *Solid State Commun.* **2005**, *136*, 333−337.

(57) Palummo, M.; Hogan, C.; Sottile, F.; Bagalá, P.; Rubio, A. *J. Chem. Phys.* **2009**, *131*.
(58) Ma, Y.; Rohlfing, M.; Molteni, C. *J. Chem. Theory Comput.* **2010**, *6*, 257−265.
(59) Rocca, D.; Lu, D.; Galli, G. *J. Chem. Phys.* **2010**, *133*, 164109.
(60) Garcia-Lastra, J. M.; Thygesen, K. S. *Phys. Rev. Lett.* **2011**, *106*, 187402.
(61) Blase, X.; Attaccalite, C. *Appl. Phys. Lett.* **2011**, *99*, 171909.
(62) Duchemin, I.; Deutsch, T.; Blase, X. *Phys. Rev. Lett.* **2012**, *109*, 167801.
(63) Baumeier, B.; Andrienko, D.; Ma, Y.; Rohlfing, M. *J. Chem. Theory Comput.* **2012**, *8*, 997−1002.
(64) Faber, C.; Duchemin, I.; Deutsch, T.; Blase, X. *Phys. Rev. B* **2012**, *86*, 155315.
(65) Duchemin, I.; Blase, X. *Phys. Rev. B* **2013**, *87*, 245412.
(66) Frisch, M. J. et al. *Gaussian 09,* Revision D.01; Gaussian, Inc.: Wallingford, CT, 2009.
(67) Zhao, Y.; Truhlar, D. G. *Theor. Chem. Acc.* **2008**, *120*, 215−241.
(68) Li, R.; Zheng, J.; Truhlar, D. G. *Phys. Chem. Chem. Phys.* **2010**, *12*, 12697−12701.
(69) Isegawa, M.; Peverati, R.; Truhlar, D. G. *J. Chem. Phys.* **2012**, *137*, 244104.
(70) Leang, S. S.; Zahariev, F.; Gordon, M. S. *J. Chem. Phys.* **2012**, *136*, 104101.
(71) Charaf-Eddin, A.; Planchat, A.; Mennucci, B.; Adamo, C.; Jacquemin, D. *J. Chem. Theory Comput.* **2013**, *9*, 2749−2760.
(72) Cossi, M.; Barone, V. *J. Chem. Phys.* **2001**, *115*, 4708−4717.
(73) Cammi, R.; Mennucci, B. *J. Chem. Phys.* **1999**, *110*, 9877−9886.
(74) Caricato, M.; Mennucci, B.; Tomasi, J.; Ingrosso, F.; Cammi, R.; Corni, S.; Scalmani, G. *J. Chem. Phys.* **2006**, *124*, 124520.
(75) Improta, R.; Scalmani, G.; Frisch, M. J.; Barone, V. *J. Chem. Phys.* **2007**, *127*, 074504.
(76) Blase, X.; Attaccalite, C.; Olevano, V. *Phys. Rev. B* **2011**, *83*, 115103.
(77) Faber, C.; Janssen, J. L.; Côté, M.; Runge, E.; Blase, X. *Phys. Rev. B* **2011**, *84*, 155104.
(78) Whitten, J. L. *J. Chem. Phys.* **1973**, *58*, 4496−4501.
(79) Valiev, M.; Bylaska, E. J.; Govind, N.; Kowalski, K.; Straatsma, T. P.; Van Dam, H. J. J.; Wang, D.; Nieplocha, J.; Apra, E.; Windus, T. L.; de Jong, W. A. *Comput. Phys. Commun.* **2010**, *181*, 1477−1489.
(80) Weigend, F. *Phys. Chem. Chem. Phys.* **2006**, *8*, 1057−1065.
(81) Bruneval, F.; Vast, N.; Reining, L. *Phys. Rev. B* **2006**, *74*, 045102.
(82) Le Bahers, T.; Adamo, C.; Ciofini, I. *J. Chem. Theory Comput.* **2011**, *7*, 2498−2506.
(83) Jacquemin, D.; Le Bahers, T.; Adamo, C.; Ciofini, I. *Phys. Chem. Chem. Phys.* **2012**, *14*, 5383−5388. Code available at Université de Nantes, http://www.sciences.univ-nantes.fr/CEISAM/erc/marches/ (accessed February 25, 2014).
(84) Pascal, S.; Haefele, A.; Monnereau, C.; Charaf-Eddin, A.; Jacquemin, D.; Le Guennic, B.; Andraud, C.; Maury, O. *J. Phys. Chem. A* **2014**, *118*, 4038−4047.
(85) The Migdal-Galitskii total energy formalism allows calculating total energies within the many-body Green's function GW approach. Work is needed along that line to better assess the gain in accuracy as compared to DFT for standard covalent systems. For a latest study, see: Caruso, F.; Rinke, P.; Ren, X.; Scheffler, M.; Rubio, A. *Phys. Rev. B* **2012**, *86*, 081102.
(86) Grossman, J. C.; Rohlfing, M.; Mitas, L.; Louie, S. G.; Cohen, M. L. *Phys. Rev. Lett.* **2001**, *86*, 472−475.
(87) Ma, Y.; Rohlfing, M. *Phys. Rev. B* **2008**, *77*, 115118.
(88) Rinke, P.; Janotti, A.; Scheffler, M.; Van de Walle, C. G. *Phys. Rev. Lett.* **2009**, *102*, 026402.
(89) Bockstedte, M.; Marini, A.; Pankratov, O.; Rubio, A. *Phys. Rev. Lett.* **2010**, *105*, 026401.